Analytical Approach for Predicting Three-Dimensional Tire–Pavement Contact Load

Jaime A. Hernandez, Angeli Gamez, Imad L. Al-Qadi, and Morris De Beer

Three-dimensional tire–pavement contact loads of two truck tires—a new-generation wide-base tire (WBT) and a dual tire assembly (DTA)—were measured and analyzed. Extreme and typical values of tire inflation pressure (552, 690, 758, and 862 kPa) and tire loading (26, 35, 44, 62, and 79 kN) were considered in the experimental program. The measurements were performed with the stress-in-motion Mk IV system at the Council for Scientific and Industrial Research in South Africa. Peak values in three directions were compared, and the importance of tangential contact stresses was highlighted. In addition, characteristic variations of the measurements in the longitudinal, transverse, and vertical directions were identified. A function depending on two regression parameters, applied load, and distance along the contact length was proposed to represent the contact load in the vertical and transverse directions. An analysis was performed on the measurements to obtain the regression parameters, and a simplified procedure was proposed to determine tire–pavement contact loads. The contact area and contact length of the WBTs and the DTA were also compared.

Every year, a considerable amount of money is spent by government agencies to restore their country's road infrastructure through maintenance and rehabilitation. These activities become more relevant as the pavement network ages. Not only does the pavement design philosophy focus on localizing damage in upper pavement layers, but it also emphasizes efficient and cost-effective maintenance and rehabilitation methods. To minimize pavement damage, several factors must be addressed during the design process, such as environmental conditions (temperature and moisture), material properties (asphalt concrete and granular), and vehicular loading (traffic level and truck loading). The transportation industry has established a detailed national climatic database and created thorough laboratory procedures to measure material properties accurately.

Tire loading is the main excitation for the pavement response; however, conventional pavement design procedures have lacked a way to simulate actual tire contact loads. Generally, tire loads are considered to be uniform and of circular shape, an assumption that could potentially underestimate pavement stresses and strains (*1–4*). Obtaining accurate strain measurement is vital because it directly affects transfer functions used in mechanistic–empirical pavement design guides. The importance of tire contact stresses has been strongly emphasized by many researchers because of their significant impact on the pavement response. Two of the main parameters of tire loading that define contact stresses are applied load and inflation pressure.

A previous study determined that inflation pressure significantly affects surface responses, especially pavement fatigue life (*1*). Another study assumed uniform contact stresses and determined that for an asphalt concrete surface thickness of less than 2 in., the tensile strain could be underpredicted by as much as half (*2*). Other researchers found that nonuniform contact stress distribution produces the highest longitudinal strain at the bottom of the asphalt concrete, whereas circular uniform loads produce the least strain (*3*). Therefore, the nonuniformity characteristic of tire contact stresses must be considered when actual tire loading conditions are simulated.

Moreover, three-dimensional (3-D) contact stresses affect the location and magnitude of the bulk and octahedral stresses and the strain energy of distortion (*5*). Research has found that the magnitude of the applied load and tire inflation pressure defines the location of the maximum response. It was also observed that 3-D contact stresses cause large tensile strain gradients (*6*). However, in relation to surface stresses, transverse contact stresses have been recognized as one of the most influential factors inducing tensile stresses, specifically that the stress state is modified close to the surface (*7*). A previous study supplemented that finding and concluded that transverse contact stresses are indeed crucial for the pavement response, especially around the tire footprint, which can be related to top-down cracking and shear flow at shallow depths (*8–15*). Transverse tensile stresses can be as high as 50% of the vertical stresses (*8*). Therefore, considering the 3-D state of the tire contact stresses will provide pavement engineers a more accurate and comprehensive understanding of pavement behavior.

Although research has demonstrated the significance of 3-D contact stresses on pavement damage and response, experimental measurement of contact stresses is not a trivial task. Over the years, a number of advanced measuring systems have been proposed. In the late 1950s, a force-measuring stud device attached to a spring system was introduced. The device deflected in the vertical and horizontal directions. The deflections were transformed into electrical signals, and electronic photographic traces were used to determine the contact forces (*16*). Moreover, the vertical deflection and the slip and chamber angles of the tires could be varied to simulate acceleration, deceleration, and free-rolling conditions (*14*). Further advancements assisted in determining friction coefficients by measuring the applied forces in each perpendicular direction (*15*).

J. A. Hernandez, A. Gamez, and I. L. Al-Qadi, Department of Civil and Environmental Engineering, University of Illinois at Urbana–Champaign, 205 North Mathews Avenue, MC-250, Urbana, IL 61801. M. De Beer, Transport Infrastructure Engineering, Council for Scientific and Industrial Research, PO Box 395, Pretoria, South Africa. Corresponding author: J. A. Hernandez, hrnndzr2@illinois.edu.

Transportation Research Record: Journal of the Transportation Research Board, No. 2456, Transportation Research Board of the National Academies, Washington, D.C., 2014, pp. 75–84.
DOI: 10.3141/2456-08

In further relating the measured contact stresses to pavements, the size and separation of the measuring pins were defined in correlation to the friction of an average asphalt concrete surface (*5, 12*). In addition, to highlight the time dependency of asphalt materials and movement of the tire load, equipment was modified to enable contact stress variation at a specific section over time and the static data along the circumference of the tire (*16*). Decades of technological modifications have led to today's advanced measurement systems, which provide highly accurate and precise experimental data. (However, this description is not intended to be a comprehensive history of systems for measuring contact stresses.)

Addressing the nonuniformity and 3-D state of contact stresses provides a more accurate representation of tire loading. However, the use of an advanced measuring system requires a considerable amount of time and money. Therefore, the need for characterizing 3-D contact stresses and analytical equations to determine contact stresses are addressed.

EXPERIMENTAL PROGRAM

Two types of tires were tested to obtain 3-D contact loading: a new-generation wide-base tire (WBT), 445/50R22.5, and a dual tire assembly (DTA), 275/80R22.5. A combination of four tire inflation pressures *S* (552.0, 690.0, 758.0, and 862.0 kPa) and five tire loads *P* (26.6, 35.6, 44.4, 62.1, and 79.9 kN) was considered.

The measurements were conducted at the Council for Scientific and Industrial Research, in South Africa, the dual stress-in-motion (SIM) Mk IV system (Figure 1*a*) was used (*17*). The equipment consisted of two SIM pad assemblies, each measuring 750 × 357 mm in nominal area. A single pad assembly of the SIM Mk IV measurement system consisted of 1,041 pins, of which a linear array of 21 was instrumented with strain gauges. The instrumented pins were arranged laterally across the SIM pad assembly, and the remainder acted as supports for the contact patch of the test tire. The conically shaped pins were 50 mm high and fixed onto a 45-mm-thick, rigid steel base plate (*5, 17*).

During the testing phase, the test tires were fixed onto the axle on the hydraulic loading test carriage of the heavy vehicle simulator (HVS Mk IV), which was positioned laterally over the dual SIM pad assemblies. To prevent the effect of lateral variation as the tires traverse the array of instrumented pins, the tires were placed approximately over the center point of the dual SIM pads. The average speed of the test tires was approximately 0.331 m/s, and the sampling frequency of the load–stress distribution in the contact patch was 1,001 Hz. Because testing was performed at a relatively low speed, the results should be applied with caution when they are utilized for other speed or rolling conditions. As the tires traveled over the dual SIM pads, the instrumented pins measured strain, which is converted to force on the basis of the previous calibration of the sensor pins. The forces were converted to effective contact stresses by using the predefined influence area of 250.28 mm^2. This area was a unique geometrical parameter for the SIM measurement system, and it was based on the assumption that the tire was smooth and in full contact with the pin (*17*). The coordinate system was defined whereby the positive *x* direction followed the travel direction (longitudinal), the positive *z* direction pointed downward (vertical), and the positive *y* direction (transverse) was dictated by the right-hand rule.

Each loading case was repeated 10 times, and the optimal 3 out of 10 repetitions were used for analysis. The optimal repetitions were selected as the ones with the reaction force from the pin measurement closer to the applied tire load. The collected data were then filtered by using a moving average with a window size of 20 measurements. Figure 1*b* shows three samples with corresponding filtered data, including details at the peak. As can be seen, the filter process slightly shifted the data; however, neither the peak value nor the contact length changed. Static tire ink imprints of the test tires were captured by using black roof paint on white paper under the heavy vehicle simulator Mk IV for visual representation of the contact area.

3-D TIRE–PAVEMENT CONTACT

3-D Loading

As previously described, the instrumented pins measure force, which is converted to stress by dividing the force by the influence area of each pin (250.28 mm^2). The influence area is calculated on the basis of the lateral separation between pins (17.0 mm center to center) and the distance between two consecutive rows of pins (14.7 mm center to center). In converting forces to stresses, the use of 250.28 mm^2 as the influence area assumes that the tire is smooth (no ribs) and is in full contact (the tire rubber covers the pin's influence area). This approach was applied to the same experimental data, and the corresponding analyses have been published (*18*).

However, these assumptions were invalid for the tires under analysis. Each tire contained a number of ribs (8 and 10 ribs for the WBT and the DTA, respectively). Moreover, each tread pattern was nonuniform. For instance, if a pin is located at a rib edge with partial contact, the area in contact between the pin and tire could potentially be half that of a pin at the middle of the rib, resulting in stress values twice those computed with 250.28 mm^2 as the contact area. To address this concern, the location of the pins as the tires traverse the measuring system must be tracked so that the appropriate and individual pin–tire contact areas can be accurately calculated for each test repetition. The task becomes even more challenging because each rib width changes with *P* and *S* variation.

As a consequence, the analysis was performed by dividing pin measurements (in newtons) by the distance between two consecutive rows of pins (14.7 mm). This approach provided variations in nonuniform force per unit length along the length of the tire *x* in the longitudinal $q_x(x)$, transverse $q_y(x)$, and vertical $q_z(x)$ directions. Dividing $q_{x,y,z}(x)$ by the appropriate influence width results in the actual contact stresses. The shape of $q_x(x)$, $q_y(x)$, and $q_z(x)$ is the same as the contact stresses; however, the unit is force over distance (newtons per millimeter).

The typical variation of $q_x(x)$, $q_y(x)$, and $q_z(x)$ over the contact length is presented in Figure 1*c*. It was observed that vertical and transverse contact stresses had similar shapes but differed mainly in magnitude and sign. However, the variation of the longitudinal contact stresses depended on the location of the rib with respect to the tire. Three local maxima were noted for the outermost rib: two negative peaks near both ends (entrance and exit) of the contact length and a positive peak in between. For the rest of the ribs, the negative peak near one end (exit) of the tire was nonexistent.

To determine the load carried by each rib P_i (i = 1 to 8 for the WBT and 1 to 10 for the DTA), $q_z(x)$ was integrated over *x*. Figure 2 presents the variation of the ratio P_i/P for three *P*-values (26.6, 44.4, and 79.9 kN) and four *S*-values. For both tires, the shape of the distribution across the tire width changed as *P* increased. If *P* was low, the center ribs carried more load than the ones at the edges of the tire (*n*-shape distribution across the patch). However, if *P* was

(a)

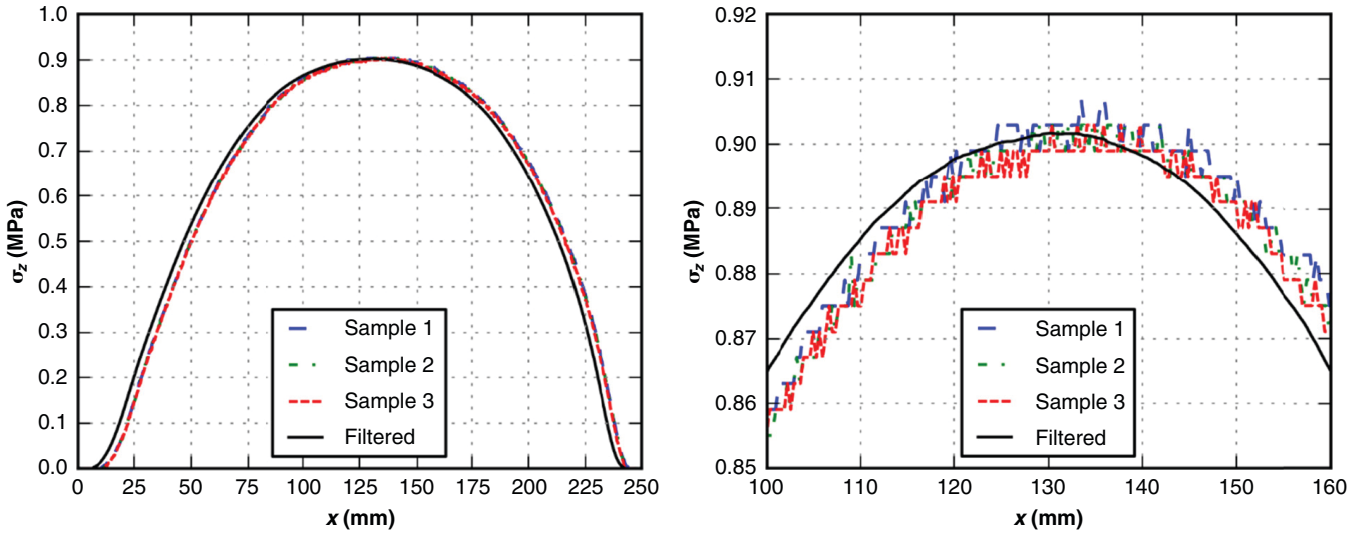

(b)

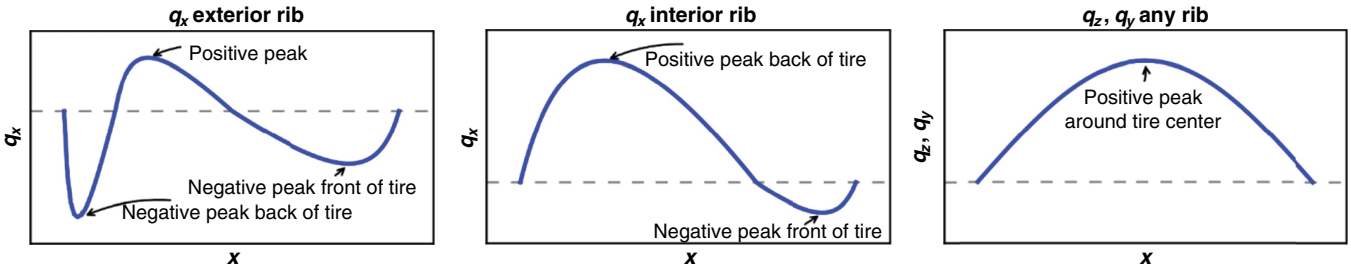

(c)

FIGURE 1 Experimental program: (*a*) measuring equipment, (*b*) moving average effect, and (*c*) typical variation of 3-D contact force per unit of contact length.

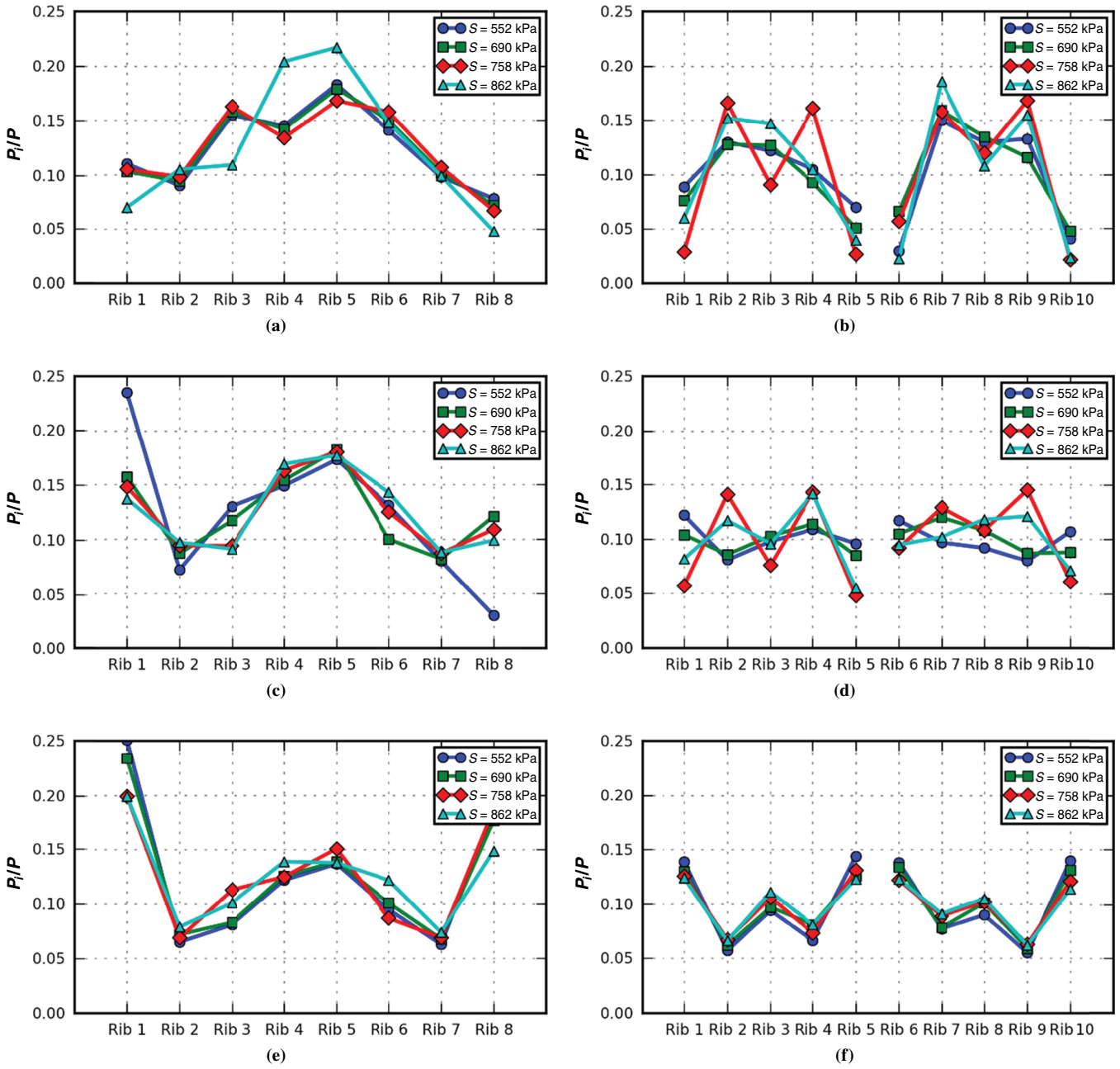

FIGURE 2 Percentage of load carried by each rib: (*a*) WBT, P = 26.6 kN; (*b*) DTA, P = 26.6 kN; (*c*) WBT, P = 44.4 kN; (*d*) DTA, P = 44.4 kN; (*e*) WBT, P = 79.9 kN; and (*f*) DTA, P = 79.9 kN.

high, the center ribs carried less load than the ones at the edges of the tire (*m*-shape distribution across the patch). The patterns were observed for all tire inflation pressure values considered in the study. As the load increased, the percentage of load carried by the edge ribs became significantly higher for the WBT than for the DTA. This finding was due to the higher number of sidewalls for the DTA compared with the WBT (four versus two). Furthermore, the variations of P_i/P across all the ribs with various S-values for the WBT were relatively close to each other for a given P-value. This finding indicated that the percentage of P carried by each rib was not significantly affected by S. For the DTA, however, the observation was valid only if the tire inflation pressure was less than or equal to 690 kPa. Finally, it was noted that P_i/P was generally higher for the WBT than for the DTA because of the lower number of ribs.

To simulate realistic contact forces and highlight three-dimensionality, the magnitudes of the measured forces in three directions were compared. Ratios of the maximum transverse $q_{y,\max}$ and longitudinal $q_{x,\max}$ forces per unit length with respect to vertical force $q_{z,\max}$ for each rib are shown in Figure 3. The horizontal axis represents the combination of the number of ribs with various S-values (e.g., for the WBT, 8 ribs by 4S equates to 32 case indicators). Contact stresses can be calculated by dividing $q_{x,y,z}$ by the appropriate influence width. Therefore, the ratios in Figure 3 are also applicable to the corresponding ratio of contact stresses.

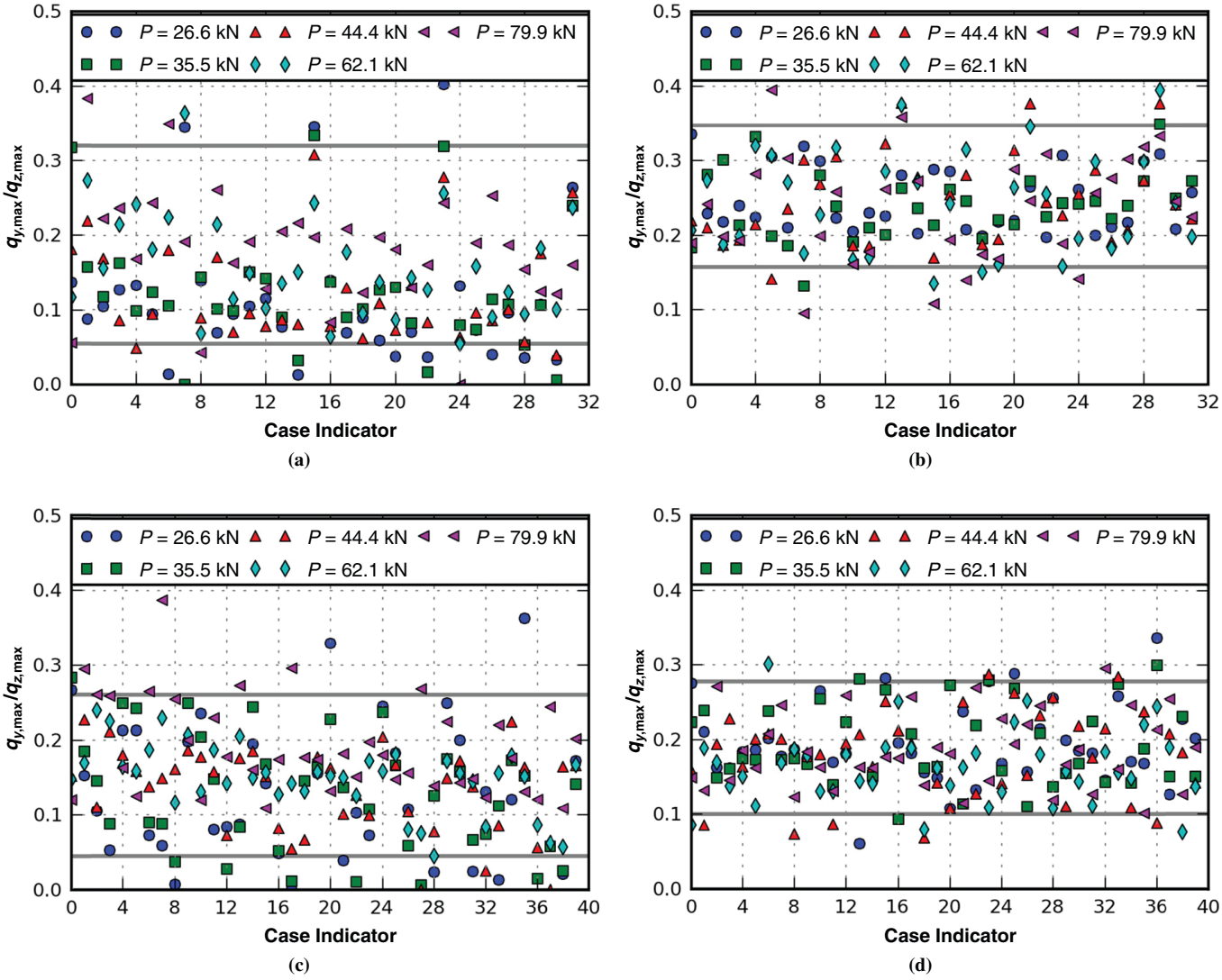

FIGURE 3 Ratios of maximum contact forces: (*a*) and (*b*) for WBT, 32 indicators, and (*c*) and (*d*) for DTA, 40 indicators.

Even though a distinct relationship between the aforementioned ratios, tire type, *P,* and *S* was not identified, two observations can be made regarding the relative magnitude of $q_{x,max}$ and $q_{y,max}$ with respect to $q_{z,max}$. On the one hand, 85% of the data points fall in the range of $0.05 < q_{x,max}/q_{z,max} < 0.32$ for the WBT, whereas the range changes to $0.05 < q_{x,max}/q_{z,max} < 0.26$ in the case of the DTA. On the other hand, the variation range for $q_{y,max}/q_{z,max}$ becomes narrower in comparison with $q_{x,max}/q_{z,max}$. The tighter band enables a greater number of data points to be considered. For the WBT, 90% of the data varies between 0.16 and 0.35, whereas the lower and upper limits change to 0.10 and 0.28 for the DTA.

From these remarks, it can be concluded that the peak transverse and longitudinal forces per unit length (or contact stresses) are relatively higher for the WBT than the DTA. In addition, regardless of the tire type, the magnitude of the tangential contact stresses is quite high, thereby gravely influencing the pavement response. Previous research has indicated the importance of considering transverse contact stresses, which have been linked to near-surface cracking and shear flow (*19*). Since ratios $q_{x,max}/q_{z,max}$ and $q_{y,max}/q_{z,max}$ are different for both tires, the same effect on the pavement response and performance may not be assumed, although both tires have the same applied load and tire inflation pressure.

Contact Area and Average Contact Length

To complete the characterization of the 3-D tire–pavement contact stresses, it was essential to obtain accurate contact area and length. The contact area was obtained from static imprints, whereas the contact length was determined on the basis of the variation of q_z. Figure 4 compares the change of the contact area *A* and the average contact length *l* of both tires. As expected, the contact area increased as *P* reached 79 kN. In addition, Ac was greater for the DTA than for the WBT for all loading cases, and the contact area ratio between the DTA and the WBT was as high as 1.3.

For the average contact length, a strong linear relationship was found when the *l*'s of both tires were compared. The average contact length for the DTA was approximately 8% shorter than the contact length for the WBT. A linear correlation was also found when the maximum contact length was compared for both tires, and it was

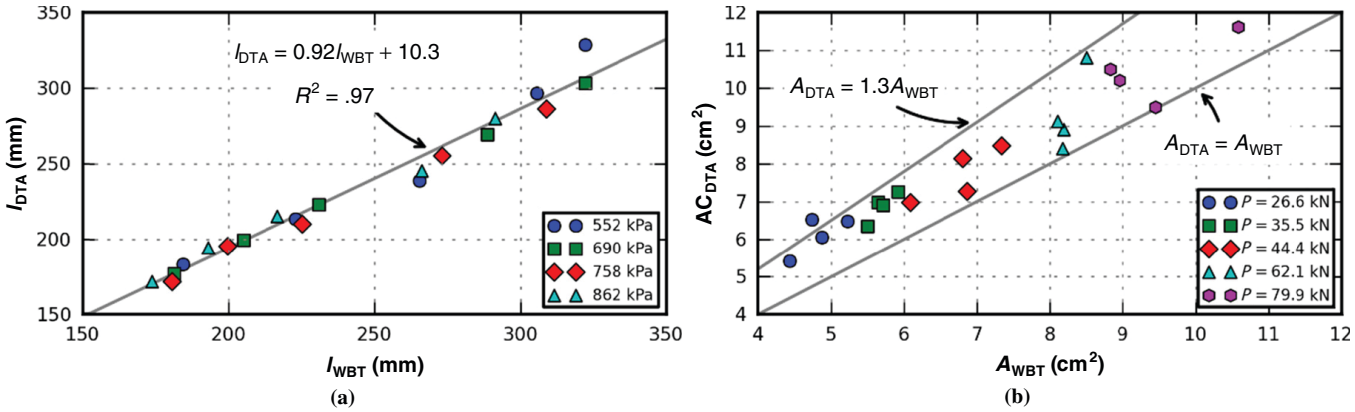

FIGURE 4 DTA versus WBT: (*a*) average contact length and (*b*) contact area (*18*).

determined that the contact length of the DTA was approximately 36% shorter (*18*).

REGRESSION ANALYSIS

A regression analysis was performed on the variation of $q_z(x)$, $q_y(x)$, and contact length for the tested tires. In the case of $q_z(x)$ and $q_y(x)$, available equations in the literature were used and corresponding regression coefficients were determined (*19*). The longitudinal contact force per unit length was not further analyzed in this study because of its particular variation (see Figure 1) and association with certain phenomena, such as tire wear and noise, more than with pavement damage. Accordingly, a linear correlation of the l with P was identified.

Contact Forces per Unit Length

As previously explained, more than one pin measured the contact forces per rib. Deriving one expression for the load variation of each pin would be impractical and would nullify the simplicity of the final result. With this aspect in mind, a single curve for each force distribution, $q_z(x)$ and $q_y(x)$, was calculated in each rib and loading case on the basis of the weighted average of the resultant force of each pin measurement:

$$\bar{q}_{zi}(x) = \frac{\sum_{j=1}^{n_j} F_{zij} q_{zij}(x)}{\sum_{j=1}^{n_j} F_{zij}}$$

$$\bar{q}_{yi}(x) = \frac{\sum_{j=1}^{n_j} |F_{yij}||q_{yij}(x)|}{\sum_{j=1}^{n_j} |F_{yij}|} \quad (1)$$

where

x = distance along contact length;
$\bar{q}_{zi}(x)$, $\bar{q}_{yi}(x)$ = average variation of vertical and transverse contact forces, respectively, per unit length with respect to x for rib i;
$q_{zij}(x)$, $q_{yij}(x)$ = variation of vertical and transverse contact forces, respectively, per unit length for pin j in rib i;
F_{zij}, F_{yij} = resultant force in vertical and transverse directions, respectively, for rib i, pin j; and
n_j = number of tire ribs (n_j = 8 for WBT and 10 for DTA).

F_{zij} and F_{yij} are calculated by integrating $q_{zij}(x)$ and $q_{yij}(x)$ over the contact length of pin j in rib i. Figure 5 shows the typical variations of $q_z(x)$ and $q_y(x)$ in one rib. The dashed lines represent the pin measurements, and the solid lines correspond to $\bar{q}_{zi}$ and $\bar{q}_{yi}$ obtained with Equation 1.

On the basis of the work by Guo and Li (*20*), it was assumed that the variation of the vertical and transverse contact forces per unit length can be expressed as follows:

$$\bar{q}_{z,y}(\xi) = \alpha \frac{P}{2a}\left(1 + \frac{1}{2n}\right)\left(1 - \xi^{2n}\right) \quad (2)$$

where

P = applied tire load (kN),
a = $l/2$ = half contact length (mm),
ξ = x/a = normalized distance along contact length, and
n, α = fitting parameters.

Nonlinear least-squares curve fitting was used to find regression parameters n and α in Equation 2 for each tire (WBT and DTA) and loading case (720 regressions).

Figure 6 presents a summary of the calculated coefficient of determination R^2. An improved fit was obtained for $\bar{q}_z$ in comparison with $\bar{q}_y$. In addition, $\bar{q}_y$ was slightly better fitted for the WBT than for the DTA. The aforementioned observations can be inferred from the fifth percentile of the plotted regression data. For the WBT, the fifth percentile for $\bar{q}_z$ and $\bar{q}_y$ is 0.96 and 0.91, respectively. In the case of the DTA, the corresponding values are 0.95 and 0.87.

After Equation 2 was fitted with experimental data, the obtained coefficients n and α were assumed to vary with P and S:

$$n = k_1 + k_2 \frac{P}{10^3} + k_3 \frac{S}{10^3}$$

$$\alpha = c_1 + c_2 \frac{P}{10^3} + c_3 \frac{S}{10^3} + c_4 \left(\frac{P}{10^3}\right)^2 + c_5 \left(\frac{S}{10^3}\right)^2 \quad (3)$$

where k_1 to k_3 and c_1 to c_5 are regression coefficients and S is in kilopascals.

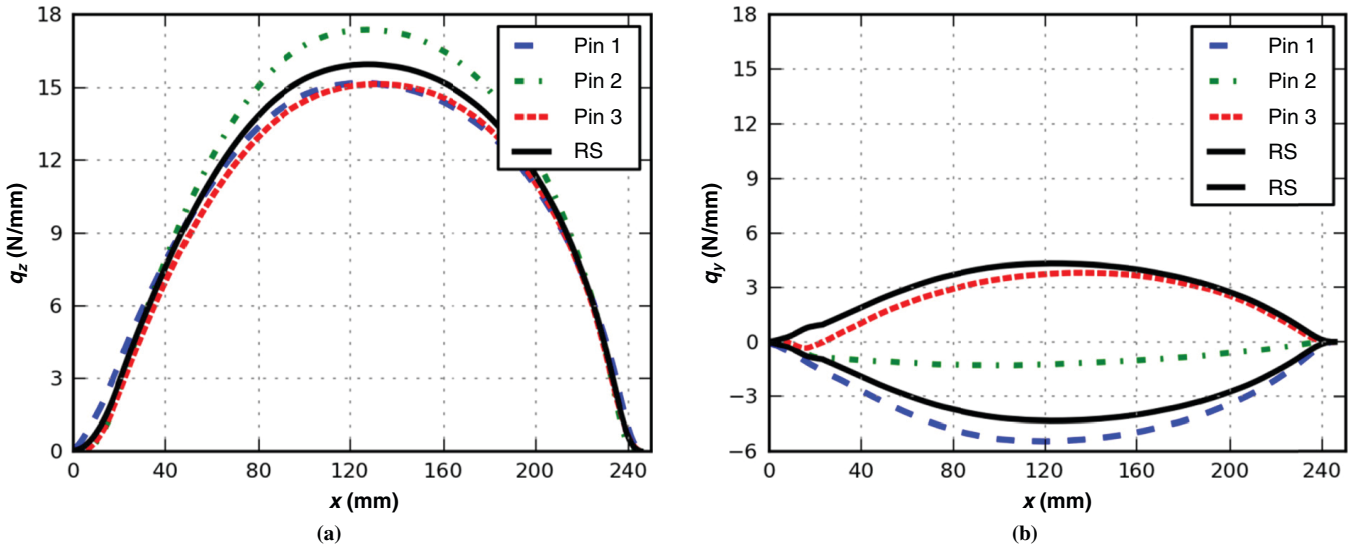

FIGURE 5 Typical variation of vertical and transverse contact force per unit length (RS = representative).

Tables 1 through 3 show the *k*- and *c*-values for *n,* α, and the corresponding R^2 of each rib. Similarly, a higher R^2 was calculated for the predicted forces in the vertical direction than in the transverse direction. The lowest R^2 in the vertical direction was .60 (Table 3, DTA, $\overline{q}_z$, Rib 4). This value is acceptable because after *P, S,* tire type, and rib number are set, $\overline{q}_z$ can be fully defined along the contact length. In the *y*-direction, some ribs have R^2-values as low as .18 (Table 3, DTA, $\overline{q}_y$, Rib 1). R^2 tends to be lower at the edge ribs compared with the ribs near the center region across the patch.

Contact Length

To determine the relationship between the contact length and the combination of various applied loads and tire inflation pressures, a procedure similar to the regression method for $\overline{q}_z$ and $\overline{q}_y$ was performed. First, it was observed that *S* did not have relevant influence on *l* (*18*), and therefore it was assumed that

$$l = d_1 + d_2 P \quad (4)$$

where d_1 and d_2 are regression coefficients.

The calculated values of d_1, d_2, and the corresponding R^2 are presented in Table 4. The lowest R^2 is .80 (WBT, Rib 5), indicating a linear relationship between *P* and *l.* In addition, the relationship is stronger for the DTA, where the lowest R^2 is .89 (DTA, Rib 1). In contrast, the variation of the R^2 throughout the ribs for the contact length is more uniform than the force distributions discussed in the previous section.

In lieu of costly and time-intensive measuring devices to determine the force–stress distribution, the established equations can be used to represent the nonuniform and 3-D state of the tire contact forces. The following is a summary of a procedure for determining the variation of contact forces per unit length and contact length:

1. Define the type of tire (WBT or DTA) and specific rib (1 to 8 for the WBT or 1 to 10 for the DTA) for which $\overline{q}_z(x)$, $\overline{q}_y(x)$, and *l* will be determined.

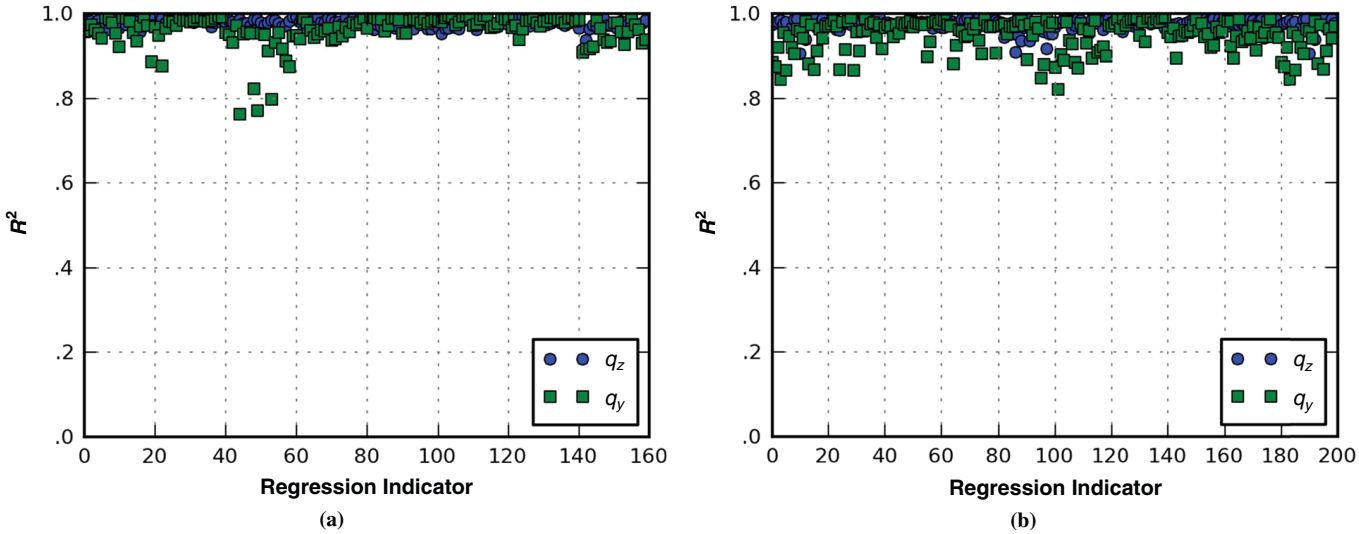

FIGURE 6 Coefficient of determination of regressions performed for (*a*) WBT and (*b*) DTA.

TABLE 1 Regression Coefficients k_1, k_2, and k_3

	WBT				DTA			
Rib	k_1	k_2	k_3	R^2	k_1	k_2	k_3	R^2
$\bar{q}_z$								
1	1.229	7.824	–0.674	.61	1.173	14.783	–1.061	.91
2	1.093	8.159	–0.567	.78	1.629	14.690	–1.474	.89
3	1.045	10.044	–0.608	.89	1.675	10.264	–1.340	.88
4	1.526	10.748	–1.152	.88	1.638	12.605	–1.426	.92
5	1.461	8.602	–1.009	.91	1.117	10.915	–0.891	.88
6	0.901	8.698	–0.476	.87	1.221	13.827	–1.162	.94
7	1.156	9.092	–0.726	.84	1.540	15.745	–1.420	.91
8	1.050	10.102	–0.745	.64	1.582	10.970	–1.271	.86
9	na	na	na	na	1.492	15.909	–1.452	.89
10	na	na	na	na	1.177	9.399	–0.896	.86
$\bar{q}_y$								
1	1.146	15.490	–0.946	.82	1.134	4.948	–0.238	.31
2	1.124	11.402	–0.889	.62	1.003	14.735	–0.994	.87
3	1.051	7.371	–0.811	.71	1.051	9.100	–0.836	.87
4	1.157	9.571	–0.927	.88	1.376	7.958	–1.081	.81
5	1.117	8.484	–0.802	.81	0.907	5.148	–0.267	.40
6	1.028	6.777	–0.647	.85	0.949	6.267	–0.192	.43
7	1.366	7.441	–0.979	.72	1.117	12.615	–0.998	.86
8	1.084	5.468	–0.487	.55	1.092	10.209	–0.944	.85
9	na	na	na	na	1.200	9.487	–0.976	.79
10	na	na	na	na	0.619	6.957	–0.056	.66

NOTE: na = not applicable.

TABLE 2 Regression Coefficients c_1 to c_5 for WBT

Rib	c_1	c_2	c_3	c_4	c_5	R^2
$\bar{q}_z$						
1	0.042	1.684	–0.073	–8.978	0.016	.89
2	0.056	–0.366	–0.025	1.280	0.038	.90
3	0.063	–0.754	0.025	3.945	–0.017	.85
4	0.096	–0.502	–0.090	2.037	0.081	.89
5	0.080	–0.729	0.003	3.243	0.006	.93
6	0.116	–0.767	–0.158	4.343	0.127	.94
7	0.025	–0.845	0.108	5.290	–0.063	.92
8	–0.008	–0.009	0.097	5.313	–0.075	.83
$\bar{q}_y$						
1	–0.016	0.294	0.067	–2.103	–0.056	.72
2	–0.010	0.448	0.023	–4.428	–0.013	.50
3	0.042	–0.254	–0.078	1.623	0.057	.73
4	0.043	–0.278	–0.085	1.938	0.068	.89
5	0.049	0.131	–0.120	–1.611	0.092	.46
6	0.011	–0.059	–0.004	–0.020	0.014	.60
7	–0.010	–0.010	0.054	–0.056	–0.036	.48
8	0.009	–0.323	0.007	3.182	–0.001	.53

TABLE 3 Regression Coefficients c_1 to c_5 for DTA

Rib	c_1	c_2	c_3	c_4	c_5	R^2
$\bar{q}_z$						
1	0.066	1.458	–0.175	–11.235	0.098	.69
2	0.091	–1.758	–0.022	13.476	0.026	.88
3	0.165	–0.769	–0.269	2.972	0.202	.72
4	–0.041	–0.777	0.279	5.559	–0.181	.60
5	0.121	0.614	–0.299	–2.971	0.189	.75
6	–0.109	1.578	0.286	–11.389	–0.210	.75
7	0.113	–2.138	–0.050	17.291	0.050	.86
8	0.047	–0.502	0.069	–0.587	–0.038	.91
9	0.022	–0.410	0.086	1.215	–0.046	.61
10	0.066	1.458	–0.175	–11.235	0.098	.69
$\bar{q}_y$						
1	0.016	–0.097	–0.019	0.970	0.010	.18
2	0.027	–0.430	–0.026	3.118	0.021	.51
3	0.018	–0.252	–0.017	2.561	0.014	.37
4	–0.011	0.013	0.050	–1.143	–0.027	.44
5	0.030	–0.148	–0.063	2.014	0.040	.85
6	–0.053	0.171	0.159	–1.503	–0.112	.39
7	0.069	–0.299	–0.158	2.224	0.117	.27
8	–0.008	–0.179	0.059	1.368	–0.040	.46
9	0.026	–0.546	–0.019	4.013	0.017	.65
10	0.016	–0.097	–0.019	0.970	0.010	.18

TABLE 4 Values of d_1 and d_2 for WBT and DTA

	WBT			DTA		
Rib	d_1	d_2	R^2	d_1	d_2	R^2
1	76.2	3.573	.81	97.7	2.741	.89
2	117.7	2.182	.85	136.9	2.085	.91
3	140.9	2.039	.82	134.4	2.094	.92
4	147.0	2.090	.82	133.0	2.113	.93
5	147.9	2.148	.80	71.7	2.997	.92
6	143.7	1.972	.82	105.0	2.594	.91
7	121.9	1.872	.85	144.1	1.992	.91
8	77.9	3.144	.85	145.6	1.876	.91
9	na	na	na	144.6	1.866	.90
10	na	na	na	66.0	3.034	.90

2. Obtain values of k_1 to k_3 and c_1 to c_5 for the variables in Step 1 from Tables 1 through 3, respectively. Recall that k_1 to k_3 and c_1 to c_5 are different for $\overline{q}_z(x)$ and $\overline{q}_y(x)$.
3. With *P, S,* and *k*- and *c*-values, calculate *n* and α by using Equation 3.
4. To compute the contact length for the specific case defined in Step 1, extract d_1 and d_2 from Table 4 and replace these values in Equation 4.
5. To calculate $\overline{q}_z$ and $\overline{q}_y$, use *P*-, *n*-, and α-values in Equation 2.

For instance, assume the input parameters are Rib 2 of the WBT with $P = 26.6$ kN and $S = 862.0$ kPa. From Table 1 the *n*-coefficients are $k_1 = 1.093$, $k_2 = 8.159$, and $k_3 = -0.567$ for $\overline{q}_z$; and $k_1 = 1.124$, $k_2 = 11.402$, and $k_3 = -0.889$ for $\overline{q}_y$. From Table 2, the α-coefficients are $c_1 = 0.056$, $c_2 = -0.366$, $c_3 = -0.025$, $c_4 = 1.280$, and $c_5 = 0.038$; and $c_1 = -0.010$, $c_2 = 0.448$, $c_3 = 0.023$, $c_4 = 4.428$, and $c_5 = -0.013$ for the vertical and transverse forces, respectively. With Equation 3,

$$n_z = 0.8212 \tag{5}$$

$$n_y = 0.6613 \tag{6}$$

$$\alpha_z = 0.0531 \tag{7}$$

$$\alpha_y = 0.0094 \tag{8}$$

Moreover, the contact length parameters are $d_1 = 117.7$ and $d_2 = 2.182$; therefore, with Equation 4, $l = 175.7$ mm. Finally, with Equation 2 the vertical and transverse contact forces per unit length are obtained:

$$\overline{q}_z(\xi) = 0.0129\left(1 - \xi^{1.642}\right) \tag{9}$$

$$\overline{q}_y(\xi) = 0.0025\left(1 - \xi^{1.322}\right) \tag{10}$$

CONCLUSIONS

Tire–pavement contact loads possess two important characteristics that significantly affect the pavement response: nonuniformity and three-dimensionality. Experimental data for two truck tires, the WBT and the DTA, were measured and analyzed to emphasize the importance of considering realistic contact loads. The ratio of transverse and longitudinal contact forces with respect to the vertical contact force was found to be higher for the WBT than for the DTA. The results also indicated high magnitudes of the transverse contact load regardless of tire type, and this finding asserts its relevance in pavement analysis.

Nevertheless, the procedure to collect a test matrix comprising various applied loads and inflation pressures at a facility is expensive. Therefore, a set of equations was proposed to represent contact loads in the vertical and transverse directions. Input parameters are tire type, applied tire load, inflation pressure, distance along the contact length, and two regression parameters. The regression analysis presented an improved fit for the vertical load scenario more than for the transverse load, which was especially apparent more for the WBT than for the DTA. Moreover, the coefficient of determination for the two regression variables used for the contact loads tended to be lower near the edge ribs compared with the middle area.

To determine contact stresses, the loads (or forces) were divided by the appropriate contact area. The regression analysis enhanced the expected linear relationship of the contact length, in which the coefficient of determination was high and uniform across the ribs. Still, the contact width could not be obtained accurately because of the complexity of the tire rib and given tread geometry. Also, the boundary of the proposed simplified procedure included two specific tire types used in the analysis and the applied load and inflation pressure value combinations. Nonetheless, this study demonstrated the feasibility of a simplified procedure for analyzing tire–pavement contact loads in the vertical and transverse directions.

ACKNOWLEDGMENTS

This paper pertains to the results of an ongoing pooled fund study, The Impact of Wide-Base Tires on Pavement—A National Study, and is based on work supported by FHWA. The project is conducted in cooperation with the Illinois Center for Transportation; FHWA, U.S. Department of Transportation; the Rubber Manufacturers Association; and the state departments of transportation in Illinois, Minnesota, Montana, New York, Oklahoma, Texas, and Virginia. This project is managed by Eric Weaver, who has been instrumental in providing direction and input. The authors greatly appreciate the feedback and input of David Lippert, Shongtao Dai, Dan Hill, Wes Yang, John Bowman, Brian Diefenderfer, and Larry Buttler.

REFERENCES

1. Kim, O. K., C. A. Bell, and J. E. Wilson. Effect of Increased Truck Tire Pressure on Asphalt Concrete Pavement. *Journal of Transportation Engineering,* ASCE, Vol. 115, No. 4, 1989, pp. 329–350.
2. Tielking, J. T., and F. L. Roberts. Tire Contact Pressure and Its Effect on Pavement Strain. *Journal of Transportation Engineering,* ASCE, Vol. 113, No. 1, 1987, pp. 56–71.
3. Siddharthan, R. V., N. Krishnamenon, M. El-Mously, and P. E. Sebaaly. Investigation of Tire Contact Stress Distributions on Pavement Response. *Journal of Transportation Engineering,* ASCE, Vol. 128, No. 2, 2002, pp. 136–144.
4. De Beer, M., J. W. Maina, Y. van Rensburg, and J. M. Greben. Toward Using Tire-Road Contact Stresses in Pavement Design and Analysis. *Tire Science and Technology,* Vol. 40, No. 4, 2012, pp. 246–271.
5. De Beer, M., C. Fisher, and F. J. Jooste. Determination of Pneumatic Tyre/Pavement Interface Contact Stresses Under Moving Loads and Some Effects on Pavements with Thin Asphalt Surfacing. In *Proceedings of the 8th International Conference on Asphalt Pavements,* Seattle, Wash., International Society for Asphalt Pavements, Lino Lakes, Minn., 1997, pp. 179–227.

6. Jacob, M.M.J., and J. Moraal. The Influence of Tyre Characteristics on the Normal Stresses in Asphalt Concrete Pavements. In *Heavy Vehicles and Road: Technology, Safety, and Policy—Proceedings of the 3rd International Symposium on Heavy Vehicle Weights and Dimensions,* Cambridge, United Kingdom, 1992, pp. 218–224.
7. Myers, L.A., R. Roque, B.E. Ruth, and C. Drakos. Measurement of Contact Stresses for Different Truck Tire Types to Evaluate Their Influence on Near-Surface Cracking and Rutting. In *Transportation Research Record: Journal of the Transportation Research Board, No. 1655,* TRB, National Research Council, Washington, D.C., 1999, pp. 175–184.
8. Al-Qadi, I.L., and P.J. Yoo. Effect of Surface Tangential Contact Stresses on Flexible Pavement Response. *Journal of the Association of Asphalt Paving Technologists,* Vol. 76, 2007, pp. 663–692.
9. Al-Qadi, I.L., H. Wang, P.J. Yoo, and S.H. Dessouky. Dynamic Analysis and In Situ Validation of Perpetual Pavement Response to Vehicular Loading. In *Transportation Research Record: Journal of the Transportation Research Board, No. 2087,* Transportation Research Board of the National Academies, Washington, D.C., 2008, pp. 29–39.
10. Wang, H., and I.L. Al-Qadi. Combined Effect of Moving Wheel Loading and Three-Dimensional Contact Stresses on Perpetual Pavement Responses. In *Transportation Research Record: Journal of the Transportation Research Board, No. 2095,* Transportation Research Board of the National Academies, Washington, D.C., 2009, pp. 53–61.
11. Al-Qadi, I.L., and H. Wang. Full-depth Pavement Responses Under Various Tire Configurations: Accelerated Pavement Testing and Finite Element Modeling. *Journal of the Association of Asphalt Paving Technologists,* Vol. 78, 2009, pp. 721–760.
12. Al-Qadi, I.L., and H. Wang. *Evaluation of Pavement Damage Due to New Tire Designs.* Publication ICT-09-048. Illinois Center for Transportation, University of Illinois at Urbana–Champaign, 2009.
13. Bonse, R.P., and S.H. Kuhn. Dynamic Forces Exerted by Moving Vehicles on a Road Surface. In *Bulletin 233,* HRB, National Research Council, Washington, D.C., 1959, pp. 9–32.
14. Lippmann, S.A., and K.L. Oblizajek. *The Distributions of Stress Between the Tread and the Road for Freely Rolling Tires.* SAE Technical Paper 740072. Society of Automotive Engineers, Washington, D.C., 1974.
15. Kulakowski, B.T. Measurement and Modeling of Truck Tire Traction Characteristics. In *Vehicle, Tire, Pavement Interface,* ASTM STP 1164, American Society for Testing and Materials, Philadelphia, Pa., 1992, pp. 112–124.
16. Koehne, S.H., B. Matute, and R. Mundl. Evaluation of Tire Tread and Body Interactions in the Contact Patch. *Tire Science and Technology,* Vol. 3, No. 3, 2003, pp. 159–172.
17. De Beer, M., and C. Fisher. Stress-in-Motion (SIM) System for Capturing Tri-Axial Tyre–Road Interaction in the Contact Patch. *Measurement,* Vol. 46, No. 7, 2013, pp. 2155–2173.
18. Hernandez, J.A., I.L. Al-Qadi, and M. De Beer. Impact of Tire Loading and Tire Pressure on Measured 3-D Contact Stresses. In *Airfield and Highway Pavement 2013: Sustainable and Efficient Pavements,* ASCE, New York, 2013.
19. Yoo, P.J., and I.L. Al-Qadi. The Truth and Myth of Fatigue Cracking Potential in Hot-Mix Asphalt: Numerical Analysis and Validation. *Journal of the Association of Asphalt Paving Technologists,* Vol. 77, 2008, pp. 549–590.
20. Guo, K., and D. Li. UniTire: Unified Tire Model for Vehicle Dynamic Simulation. *Vehicle System Dynamics,* Vol. 45, 2008, pp. 79–99.

The Flexible Pavement Design Committee peer-reviewed this paper.